The Minnesota Scanner: A Prototype Sensor for Three-Dimensional Tracking of Moving Body Segments

BRETT R. SORENSEN, MAX DONATH, MEMBER, IEEE, GUO-BEN YANG, STUDENT MEMBER, IEEE, AND ROLAND C. STARR, MEMBER, IEEE

Abstract—**An advanced method of tracking the three-dimensional motion of bodies has been developed. This system, which is presently being used for human motion tracking, has the potential for dynamically characterizing robot motion and also provides a means for facilitating robot endpoint control. Three rotating planes of laser light, fixed and moving photovoltaic diode targets, and a pipelined architecture of analog and digital electronics are used to locate multiple targets whose number is only limited by available computer memory. Data collection rates are a function of the laser scan rotation speed and are currently selectable up to 480 Hz. The tested performance on a preliminary prototype designed for 0.1-in accuracy (for tracking human motion) at a 480-Hz data rate includes a resolution of 0.8 mm (0.03 in), a repeatability of ±0.635 mm (±0.025 in), and an absolute accuracy of ±2.0 mm (±0.08 in) within an eight cubic meter volume with all results applicable at the 95-percent level of confidence along each coordinate direction. The system can be used to reduce *XYZ* target position data to body angular orientation which, for this first prototype, ranges in accuracy from ±0.5° to ±1°. Moving targets can be tracked at speeds exceeding 1 m/s with signal integrity tested but not limited to 25-Hz motions.**

INTRODUCTION

SENSORS that track body motion are needed for implementing closed-loop motion control of multi-degree-of-freedom systems and for analyzing their dynamics. Many potential applications exist, ranging from the analysis of human motion to the control of robot motion. In the case of robots, positioning accuracy and fast response of end-effector motion are important for many applications. While industrial robots have acceptable repeatability, their absolute positioning accuracy is relatively poor. This is for the most part due to their control architecture which involves sensing and feedback of position and velocity at the joint level rather than at the end-effector level. Traditional inverse kinematics-based strategies for robot joint motion control do not accommodate for large, cross-coupled, dynamic effects that can occur.

A variety of control strategies have been proposed for improving robot performance where larger payloads must be moved at reasonably high speeds. Such strategies are based on feedback from sensors which directly measure the motion to be controlled. For example, the performance of the inverse dynamics or computed torque approach extensively described in the robotics literature [4] would be significantly improved if a sensor were available for tracking the actual Cartesian motion (6 degrees of freedom) of the end-effector carrying a payload. Other methods such as the operational space formulation [6] and CMAC [10] can also take advantage of such sensors. For example, Miller [10] describes a CMAC-based strategy for controlling the location of the end-effector relative to sensor-monitored landmarks in the task environment. Our objective in exploring the sensor described in this paper is to locate the effector with respect to a global fixed world coordinate system. Sensing relative displacements among multiple objects is subsumed.

Further applications include the control of robots exhibiting flexibility in their joints or in their structure. Such systems assume the availability of sensors which can accurately track the full 6 degrees of freedom of end-effector motion in order to facilitate what is known as endpoint control [14].

A number of instrumentation systems have been developed for measuring three-dimensional (3-D) body motion, in particular for the study of human movement. These include systems based on photogrammetry, electrogoniometry, sonic triangulation, accelerometry, and electrooptical phenomena. During the last decade, particular attention has been focused on electrooptical techniques. Within this group are several systems currently used in human motion laboratories: VICOM, SELSPOT, WATSMART, and the United Technologies systems. All these systems calculate the position of a target point from its image coordinates in two or more camera reference frames. The targets are either LED's and the cameras are large linear area lateral photo-effect diodes (SELSPOT and WATSMART), or reflective markers are used as targets with video cameras (VICOM) or digital cameras (United Technologies) for data acquisition. Each of these systems quote comparable performance characteristics, sufficient for the purpose of collecting human motion data, but each

Manuscript received July 21, 1987; revised January 30, 1988. This work was partially supported by the National Institute for Disability Rehabilitation and Research REC under Grant G008300075, the National Science Foundation PYI Award under Grant DMC-8351827, and the University of Minnesota. Part of the material in this paper was presented at the IEEE International Conference on Robotics and Automation, Raleigh, NC, March 1987.

B. R. Sorensen was with the Department of Mechanical Engineering, University of Minnesota, Minneapolis, MN 55455. He is now with the U.S. Army Ballistics Laboratory, SLCBR & TB-P, Arlington Proving Grounds, MD 21005.

M. Donath and G. B. Yang are with the Department of Mechanical Engineering, University of Minnesota, Minneapolis, MN 55455.

R. C. Starr was with the Department of Mechanical Engineering, University of Minnesota; Minneapolis, MN 55455. He is now with the Motion Analysis Laboratory, Gillette Childrens' Hospital, St. Paul, MN 55101.

IEEE Log Number 8928894.

1042-296X/89/0800-0499$01.00

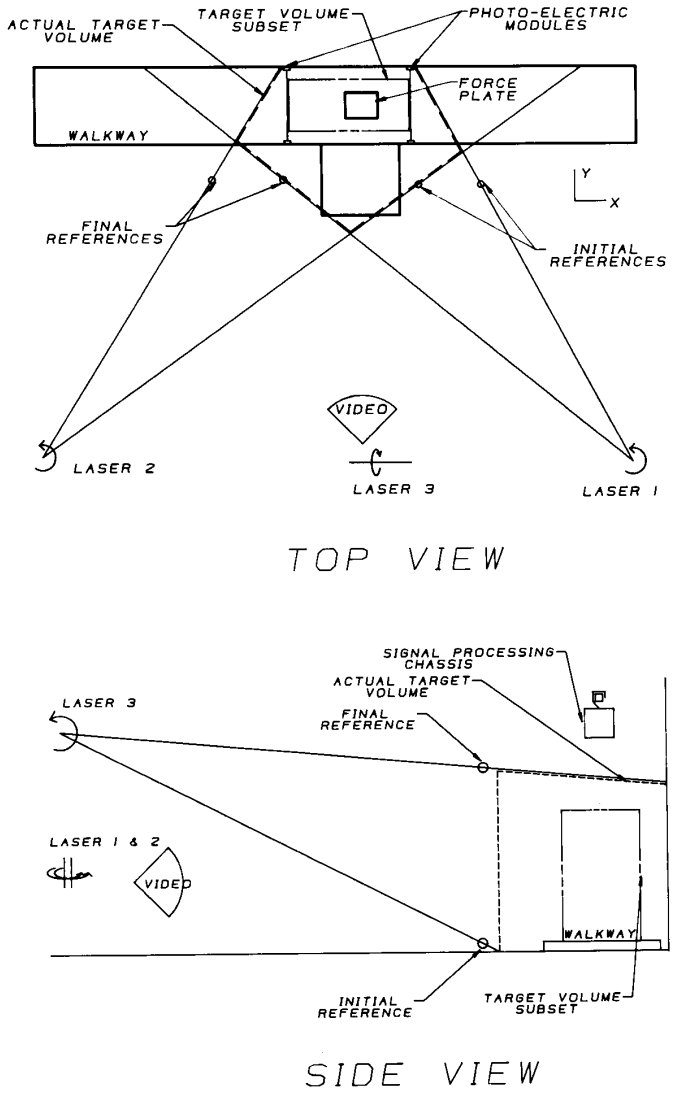

Fig. 1. Physical layout of the laboratory.

has inherent limitations in the maximum number of targets, in data processing time, in accuracy, or in bandwidth, which thus limit their utility. An extensive review of tracking systems is contained in Antonsson and Mann [1]. Systems [3], [11] have been developed for performance measurement of robot function but these are typically not compatible with closed-loop control oriented sensing. Those that are [5] have other constraints.

The system described here, the Minnesota Scanner (or MnScan), has been under development for several years in an attempt to provide a cost-effective, high-performance alternative. Our present prototype, originally developed for tracking human motion with a goal of achieving 0.1-in accuracy per axis for all three dimensions, has undergone extensive testing and calibration.

Fig. 1 shows the physical layout of the system in our Human Motion Laboratory. This paper reports on our most recent results with MnScan which demonstrate that, with appropriate redesign, the system has potential for serving as a robot endpoint sensing system.

System Configuration

The system is based on the concept that three planes of light, with differing normal vectors, intersect at a point in 3-D space. The basic premise of the method is that three intersecting planes define a point provided that none of the directional cosines of the three planes are the same. Thus if the equations of three planes are known, the intersection point's coordinates can be found.

The planes are generated by passing light from a low-power laser through a cylindrical lens arrangement and are swept through the measurement field by reflecting the planes off of mirrors rotating at constant angular velocity. The eight-mirrored surfaces of three octagonal prisms are rotated by

three 60-Hz reluctance synchronous motors. Such motors facilitate constant angular velocity and a constant phase relationship with the motor housing. This allows for a high data collection frequency, 480 Hz, and precludes the need for phased-lock loops and connections between the motors. Although the use of motors incorporating closed-loop speed control is possible, it was deemed unnecessary, given the desired specifications. As the plane moves through the workcell, it passes over photodetectors sensitive to the laser's wavelength. The signal from each detector is filtered to remove background light, amplified, and then further conditioned to provide a TTL pulse each time a plane passes over it. In our present configuration only one laser is in the volume at any one time. This is done by phasing the three mirror scan motors appropriately. This phasing, its effects, and other design issues, are discussed in more detail in Macfarlane [8] and Macfarlane and Donath [9].

Three fixed initial references are located at one corner (lower right front) of the field so that each of these detectors views only one laser. The pulses generated by these three detectors are used to initialize a master clock counter each time a laser passes over its associated initial reference detector. In addition to the initial references, there are also the multiple target photo-detectors, which are free to move within the target volume. Each time a target detector "sees" a plane, the current counter value is placed in one of three 16-bit registers associated with each detector, one register per laser source. These registers are memory mapped into the CPU's address space. Thus each register is continuously loaded with data from the clock, independent of the host processor and independent of all other targets, as often as its associated light plane passes through the target volume. The value in the register represents the time for the plane to rotate from reference to target, and can be converted to an angle since the angular velocity is constant.

The System Equations

In order to compute a target's location, the locations of the reference targets and the optical axes of rotation must be known. During the calibration process, the axes of rotation are positioned so that they are parallel or orthogonal to each other and the global coordinate system (GCS), with two axes being vertical and the third, horizontal in orientation. This is done to simplify the position calulations. The simplification is necessary in order to decrease the computational time required for data reduction. Bechtold [2] showed that if the axes of rotation were arbitrarily located, the solution process would be an open-form iteration. By orthogonalizing the axes of rotation, the solution process becomes closed-form in nature and thus facilitates real-time computation.

In order to first locate a moving target in a two-dimensional (2-D) plane, a photodetector is needed as a starting reference point for each laser. A schematic model of laser 1 and 2 in the X–Y plane is shown in Fig. 2(a), where A, B represent the optical axes of rotation for lasers 1 and 2 (light sources), T is the target position to be measured, S_i is the starting reference point for laser i (i = 1, 2), angles θ_1, θ_2 are fixed for the system, and α, β are computed based on the elapsed time from

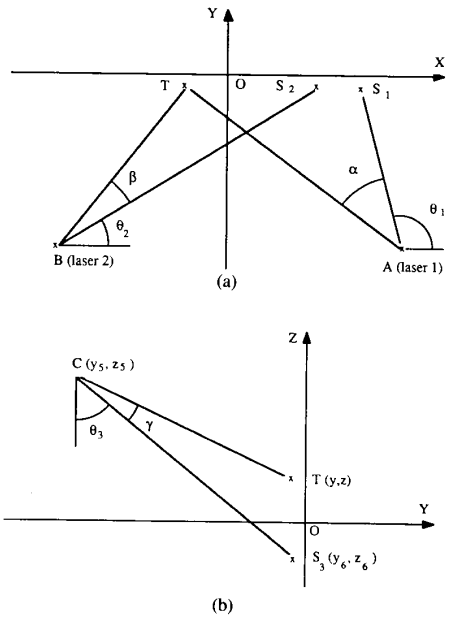

Fig. 2. (a) Schematic model of lasers 1 and 2 in the X–Y plane. (b) Schematic model of laser 3 and target T in the Y–Z plane.

the initial reference detector "hit" to the target detector firing and on the angular velocity of the passing beam.

Let the x, y coordinates of these points be $A(x_1, y_1)$, $B(x_2, y_2)$, $S_1(x_3, y_3)$, $S_2(x_4, y_4)$, and $T(x, y)$. We can then compute the position of target T as

$$x = \frac{1}{C_1 - C_2}\,(C_1x_1 - C_2x_2 - y_1 + y_2)$$

$$y = \frac{1}{C_1 - C_2}\,(C_1C_2x_1 - C_1C_2x_2 - C_2y_1 + C_1y_2) \qquad (1)$$

where

$$C_1 = \frac{(y_3 - y_1) + (x_3 - x_1)\tan\alpha}{(x_3 - x_1) - (y_3 - y_1)\tan\alpha}$$

$$C_2 = \frac{(y_4 - y_2) + (x_4 - x_2)\tan\beta}{(x_4 - x_2) - (y_4 - y_2)\tan\beta}. \qquad (2)$$

To determine the third coordinate z of the target position, we define $C(y_5, z_5)$ to be the optical axis of rotation for laser 3 (light source), $T(y, z)$ is the target position to be measured, $S_3(y_6, z_6)$ is the starting reference for laser 3, θ_3 is a fixed angle, and γ is the rotating angle determined as before for α and β (see Fig. 2(b)).

Thus the coordinate z can be obtained as

$$z = C_3(y - y_5) + z_5 \qquad (3)$$

where

$$C_3 = \frac{(z_6 - z_5) + (y_6 - y_5)\tan\gamma}{(y_6 - y_5) - (z_6 - z_5)\tan\gamma}. \qquad (4)$$

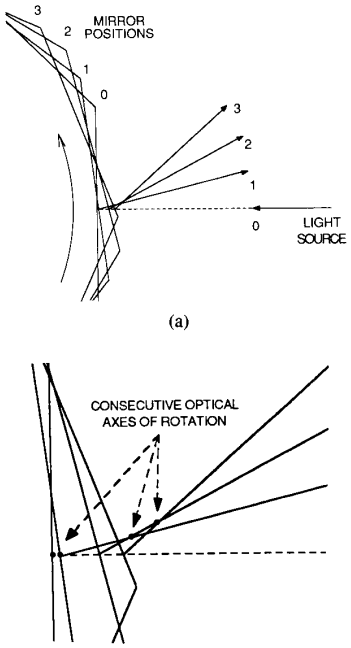

Fig. 3. (a) Reflected light beam motion for consecutive scan mirror positions. (b) Blowup of region adjacent to the impingement of the light source on the scan mirror.

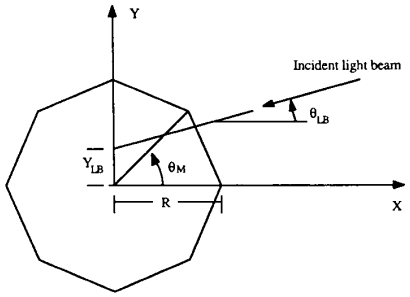

Fig. 4. Definition of parameters for finding the moving axis of rotation.

Moving Axis of Rotation

Although the use of the octagonal mirror gives the system a high bandwidth, it introduces a complication. Since the reflective surface is a finite distance from the mechanical axis of rotation, the optical and mechanical axes are not coaligned, and as a result, the optical axis is not fixed in space, but moves as the mirror rotates (see Fig. 3(a) and (b)). This motion is not negligible and cannot be ignored since the axis can move as much as 0.25 in in each direction perpendicular to the axis of rotation. Fortunately, this motion is a function of realizable parameters and can be described by a set of equations for the coordinates which are functions of the mirror rotation angle θ_M, the orientation of the incident light beam θ_{LB}, and the prismatic radius R (see Fig. 4).

$$x(\theta_M) = -\frac{[R\cos(3/8\pi)\cos(\theta_{LB}-\theta_M-3/8\pi)+y_{LB}\cos(\theta_{LB})]\cos(2\theta_M-\theta_{LB}-1/4\pi)}{\tan(\theta_{LB}-\theta_M-3/8\pi)}+u\cos(\theta_{LB}) \quad (5)$$

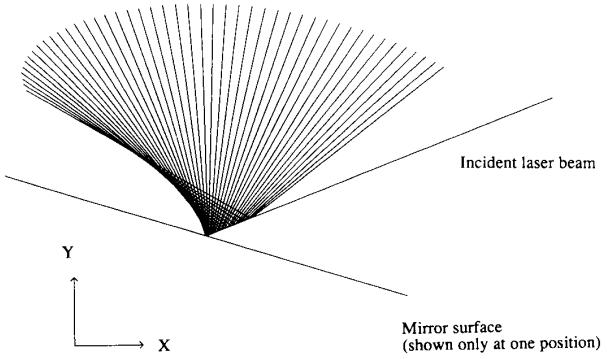

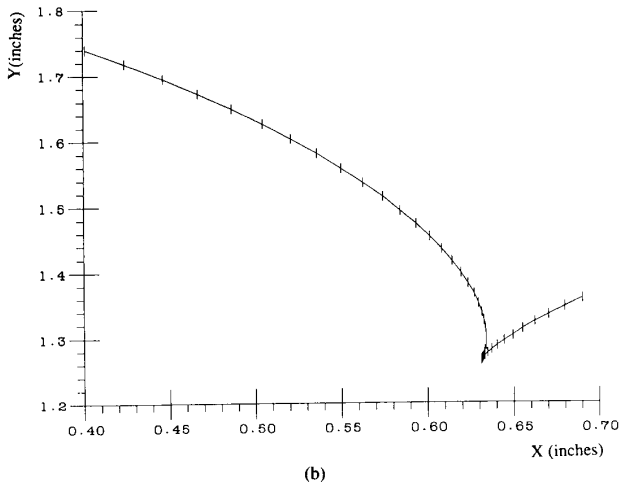

Fig. 5. (a) Reflected light planes for successive one-degree rotations of the mirror. (b) The moving optical axis of rotation for one degree increments.

$$y(\theta_M) = y_{LB} + u\sin(\theta_{LB}) - [x(\theta_M) - u\cos(\theta_{LB})]\tan(2\theta_M-\theta_{LB}-1/4\pi) \quad (6)$$

where

$$u = -\frac{R\sin(3/8\pi)+y_{LB}\cos(\theta_M+3/8\pi)}{\sin(\theta_{LB}-\theta_M-3/8\pi)}. \quad (7)$$

These equations were developed based on differential geometry and describe the locus of points traced out by the intersection of consecutive reflected light beams (see Fig. 5). More importantly, it can be proved that

$$\|\phi\| = \|2\theta_M - 2\theta_{LB} - 1/4\pi\| \quad (8)$$

where ϕ is the optical angle of rotation. This is important since it signifies that if the mechanical angular velocity of the prismatic mirror is constant, then the angular velocity of the rotating light beam must be constant. Furthermore, the optical angular velocity is twice the mirror's rotational velocity. Since

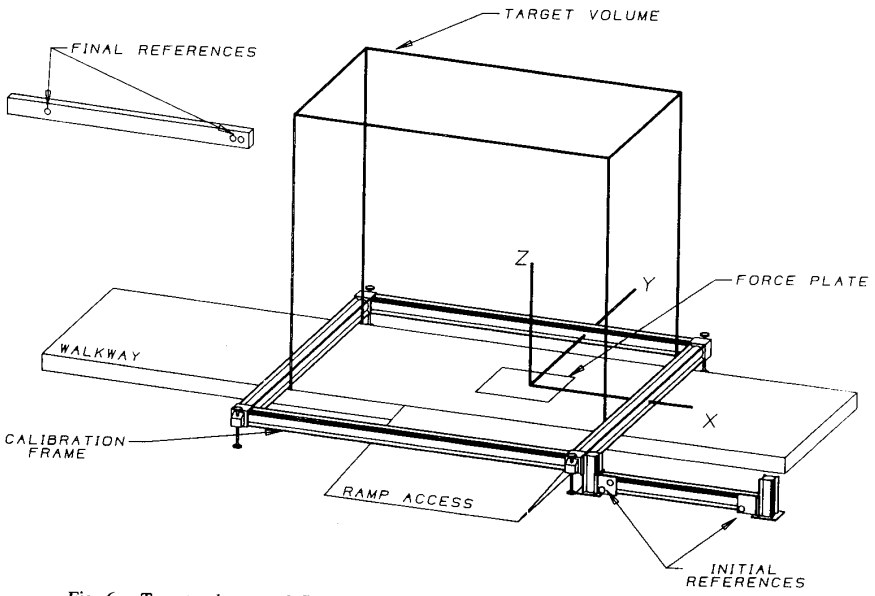

Fig. 6. Target volume as defined by the inertial reference and the global coordinate system.

the effective region of interest is the upper left-hand portion of the curve as shown in Fig. 5(b), a linear approximation is quite sufficient.

Target Configuration

Target photodetectors were selected to have high sensitivity in order to minimize needed laser power, and have a 120° wide angle field in order to be visible to all lasers throughout the field. The active area of the sensor is 20 mm^2.

As stated, each target detector defines a point in space. To define the orientation of a body, a minimum of three points is required. A fourth point provides redundancy in the event that one detector is momentarily blocked from the view of the light planes, and also allows a least squares estimate to be fitted based on four sets of three points. The greater the separation distance between targets, the greater the accuracy in determining the body orientation. However, in order for the target mounts not to get unwieldy, the separation distance was constrained.

Determination of System Parameters

As indicated earlier, the location of each axis of rotation must be determined in order to effectively use the system. Other parameters that must be identified are the location of the initial and reference photodetectors for each laser. To locate the positions of the three fixed reference diode targets and a local coordinate frame for each moving axis of rotation, a Zeiss precision measurement system was used. This measurement device consists of two theodolites interfaced to a computer. Once the theodolites are calibrated to provide their locations with respect to a global coordinate frame in the room, points can be located with respect to the defined frame with accuracy and repeatability better than 0.003 in.

To do the system calibration, four or more points of known location are needed to calibrate the theodolites. These points were located on an optical bench (2 m × 2 m) which straddled the target volume during the calibration process (see Fig. 6). This removable test bench was used to define the global coordinate system and to set up the Zeiss calibration points which were located with a 6-ft vernier caliper. Using this system, the three mechanical axes of rotation and the three reference detector locations were measured. With these system parameters determined, the data generated by the system can be reduced to 3-D points.

System Configuration Effects on Accuracy

A sensitivity analysis can be performed in order to determine the effects of individual parameters on the overall system performance. For the 2-D case from Fig. 2(a) as well as (1) and (2), the overall error in the coordinates x and y of the target T due to an error in each parameter can be expressed as the effects imposed by each of the two lasers.

$$\Delta x = \Delta L_1 + \Delta L_2$$

$$\Delta y = C_2 \Delta L_1 + C_1 \Delta L_2 \tag{9}$$

where the effect of laser 1, ΔL_1, and the effect of laser 2, ΔL_2, are

$$\Delta L_1 = \frac{1}{(C_1 - C_2)^2} (-C_2 x_1 + C_2 x_2 + y_1 - y_2) \Delta C_1$$

$$\Delta L_2 = \frac{1}{(C_1 - C_2)^2} (C_1 x_1 - C_1 x_2 - y_1 + y_2) \Delta C_2 \tag{10}$$

and

$$\Delta C_1 = \frac{\text{Sec}^2\ \alpha}{[(x_3 - x_1) - (y_3 - y_1)\ \tan\ \alpha]^2}$$
$$\{(y_3 - y_1)(\Delta x_1 - \Delta x_3) - (x_3 - x_1)(\Delta y_1 - \Delta y_3) + [(x_3 - x_1)^2 + (y_3 - y_1)^2]\Delta\alpha\}$$

$$\Delta C_2 = \frac{\text{Sec}^2\ \alpha}{[(x_4 - x_2) - (y_4 - y_2)\ \tan\ \beta]^2}$$
$$\{(y_4 - y_2)(\Delta x_2 - \Delta x_4) - (x_4 - x_2)(\Delta y_2 - \Delta y_4) + [(x_4 - x_2)^2 + (y_4 - y_2)^2]\Delta\beta\}. \quad (11)$$

The x, y coordinates for points A, B, S_1, S_2, were measured in our laboratory using the theodolites and were found to be $A(140.981, -171.272)$, $B(-221.803, -168.097)$, $S_1(49.042, -1.088)$, $S_2(10.539, -1.116)$ with all units in inches. Assuming the x, y coordinates of the target T is $(-30, 0)$ we have

$$\Delta x = -0.314\Delta x_1 + 0.120\Delta x_2 + 0.831\Delta x_3 + 0.363\Delta x_4 + 0.068\Delta y_1 - 0.008\Delta y_2 + 0.447\Delta y_3 - 0.507\Delta y_4 - 182.84\Delta\alpha - 180.000\Delta\beta$$

$$\Delta y = -0.0295\Delta x_1 - 0.121\Delta x_2 + 0.780\Delta x_3 - 0.364\Delta x_4 + 0.064\Delta y_1 + 0.008\Delta y_2 + 0.420\Delta y_3 + 0.508\Delta y_4 - 171.68\Delta\alpha + 180.36\Delta\beta. \quad (12)$$

This analysis shows that when considering all possible sources, the sensitivity of the (x, y) target coordinates to errors in the system parameters was less than unity for all but the rotation angles, α and β, for which the sensitivity is significantly larger. An error of 1 arc second, equivalent to approximately 3 clock counts (see (13) below), in *both* rotation angles, α and β, would cause a 0.1-in error in the x direction (while this same error would only lead to minimal error in the y-direction). Similar results apply for the computation of the third coordinate.

Static Performance Testing

To determine if the data generated by the system are accurate, a detailed calibration was performed. The process involved moving a vertically oriented, linear array of eight targets through the target volume.

The optical bench was used as a means for mounting and providing regular movement of the target configuration. A movable horizontal rail was placed parallel to the x axis to yield changes in y. Displacement of a vertical rail with the attached target configuration yielded changes in x. With the eight targets at varying heights, it was not necessary to change the z component. The targets were moved along 6-in intervals in the x and y directions by the appropriate adjustment of the horizontal and vertical rails. This protocol yielded data on 616 discrete points within the target volume; eleven locations in the x direction, seven in the y, and eight in the z. At each location, data were recorded using both systems; the theodolite-based method and the MnScan approach. Each target was sampled (measured) 200 times by the MnScan system to provide data for statistical analysis.

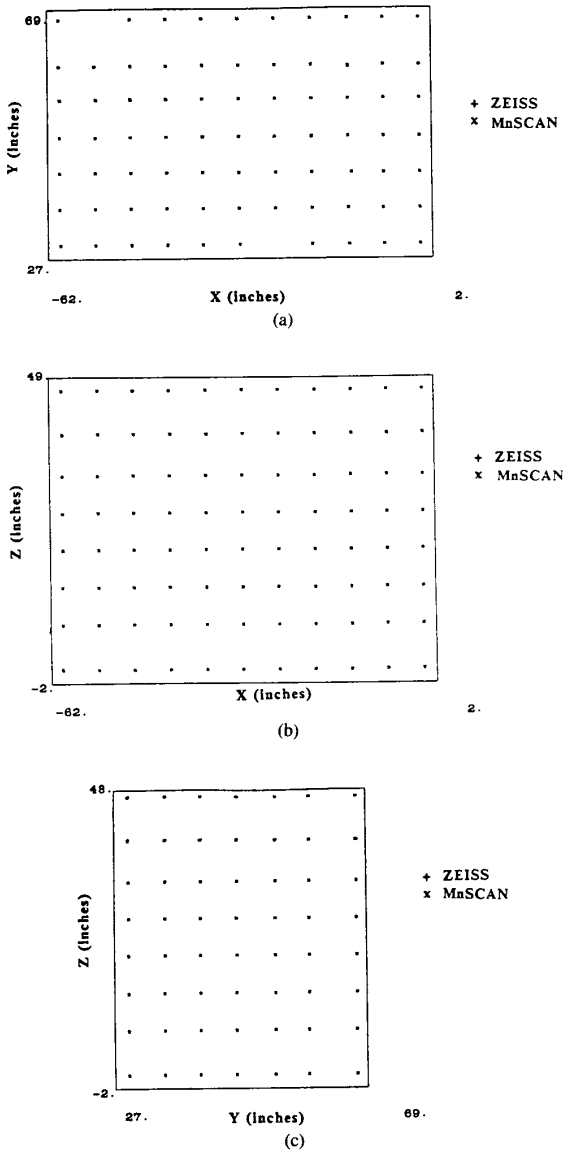

Fig. 7. (a) Plot of actual and measured points in the XY plane after the angular correction. (b) Plot of actual and measured points in the XZ plane after the angular correction. (c) Plot of the actual and measured points in the YZ plane after the angular correction.

Results

Accuracy

In testing the system, a phase lag error was discovered. By modeling the error, based on a smaller subset (200 out of 616) of the total measurement, the phase lag was eliminated. The spatial locations of the detectors for the Zeiss and the MnScan systems are shown in Fig. 7 for 3 slices through the field. It can be seen that on the scale of these plots, the data from the

two systems effectively superimpose. However, further analysis shows that there was a root mean squared error of 0.04 in. that remained and that a 95-percent confidence interval includes an error of ±0.08 in. along each axis. These results were obtained at 480-Hz data acquisition rates. (Two data points are missing from Fig. 7(a) because their associated data file was irretrievably lost by an inadvertent deletion. These were thus not included in any error or calibration analyses.)

Resolution

The spatial resolution is dependent on the position within the target volume. The input parameters to the solution equations, the three rotation angles, have an angular resolution; thus the distance from the target to each laser affects the tangential resolution of each target.

Each angle has a resolution determined by the angular velocity of the mirror and the clock speed on the data collection board. The angular resolution is the amount of rotation per clock count. For the present configuration, with an eight-faceted mirror rotating at 60 Hz and an 8-MHz clock, the resolution is

$$\frac{\left(90\,\frac{\text{degrees}}{\text{facet}}\right)\times\left(8\,\frac{\text{facets}}{\text{revolution}}\right)\times\left(60\,\frac{\text{revolutions}}{\text{second}}\right)}{8E6\,\frac{\text{counts}}{\text{second}}} = 0.0054\,\frac{\text{degrees}}{\text{count}}. \quad (13)$$

At a distance of 30 ft (the maximum target distance for any laser) the angular resolution corresponds to a tangential resolution of 0.034 in. By using the tangential resolution and the system's geometry, the actual spatial resolution at a point can be determined. This resolution has components along each of the three different axes which vary across the measurement field from half to two-thirds of the above tangential resolution of 0.034 in.

Signal-to-Noise Ratio

Noise in the signal comes from a variety of souces including electronic, optical, and environmental effects. The timing data from a single stationary detector for one laser exhibit a variation of up to five counts about a mean value; the closer to the initial reference, the smaller its effect on the overall position error. To determine the impact of this noise, data were collected at 480 Hz to allow processing by a 10-bit FFT (fast Fourier transform) for signal decomposition. The resulting power spectral density contained a large component at dc and two much smaller components at 60 and 120 Hz. The 60- and 120-Hz peaks had magnitudes of 0.0001 and 0.0003 of the 0-Hz component, respectively. This result is the same throughout the field for each plane of light, independent of detector and signal processing channel. The source of this noise has been identified, and we are working towards eliminating it.

Scatter Plots

To examine the noise effects on accuracy and resolution, a set of data (450 samples at 480 Hz) was collected for a stationary target and reduced to (x, y, z) coordinates. These data can be viewed in two planar projections (Fig. 8), an (xy) plane view and a (yz) plane view. The (xz) plane is not used because x and z are independent; the plot of this projection would just show up as a cloud of points. An important fact to remember is that the active area of the detector is 20 mm^2, or 0.176 in in the x and z directions.

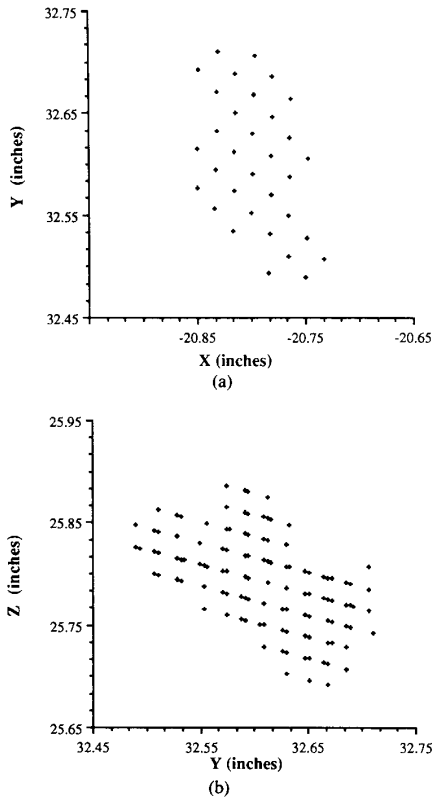

Fig. 8. (a) Scatter plots of the signal noise effects in the (xy) plane. (b) Scatter plots of the signal noise effects in the (yz) plane.

The planar projections (Fig. 8) show the effect of the 5 to 10 counts of noise at a particular spatial location within our field. In both projections patterns are visible. For the (xy) plane, computed locations exist only at the intersections of a diamond-shaped grid. This occurs because the rotating light planes from lasers 1 and 2 pass the detector at discrete values associated with the clock resolution. The diagonal lines of the grid represent the orientation of the light plane at each discrete value. Similarly, the (zy) projection shows points lining up along the direction of the light plane from laser source 3 and also in vertical lines which represent the intersection of the light planes from laser sources 1 and 2. The error over the test region falls within ±0.08 in at the 95-percent level of confidence, well within the design specifications for this prototype.

Although these projections show the locations of each digitized point, no information on the relative density of points is apparent because multiple points are superimposed. Note that in the (xy) projection of Fig. 8 only a small percentage of

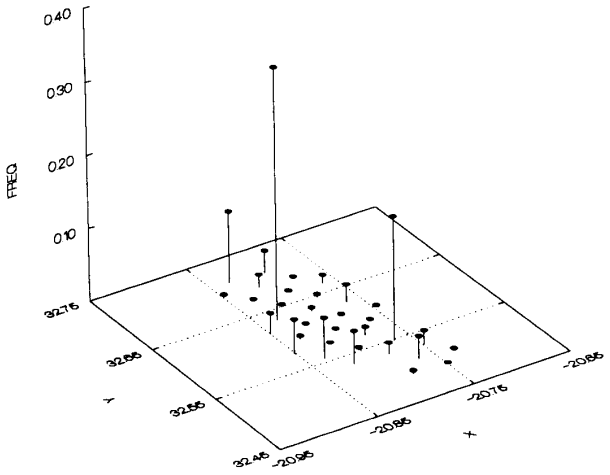

Fig. 9. Histogram of (xy) plane scatter plot.

the data points are visible. To determine the distribution of the computed position, a 2-D histogram of the (xy) scatter plot was made (Fig. 9). This graph shows that most of the points fall in a smaller region.

To examine low-pass effects on the accuracy and repeatability, the timing data were passed through a digital filter. The filter used was a tenth-order Butterworth low-pass with time reversal to preserve phase. To prevent start-up oscillations, the first half of the signal is folded and inverted about the beginning of the signal and likewise for the second half of the signal. This allows smooth transition signals and any start-up disturbances should die out in the artificial portion of the signal. To provide design variability, the -3-dB cutoff level can be specified to achieve the desired performance. To eliminate the 120-Hz peak, both 100- and 40-Hz -3-dB cutoff filters were used. Each of 27 sets of timing data (3 registers per each of 9 detectors, the intial reference and 8 targets) was passed through each filter and then rounded off to preserve the discrete nature of the data for this example. At this point, the filtered timing data can be reduced to coordinates and plotted. The resulting scatter plot based on using a filter with a -3-dB cutoff level of 40 Hz is shown in Fig. 10(a) for the xy plane and in Fig. 10(b) for the yz plane. The histogram of Fig. 10(c) confirms that the filter reduces the group of points to within a range of 0.04 in in the x and y directions or an error of ± 0.02. The same process yields a range of 0.06 in in the z direction (error of ± 0.03).

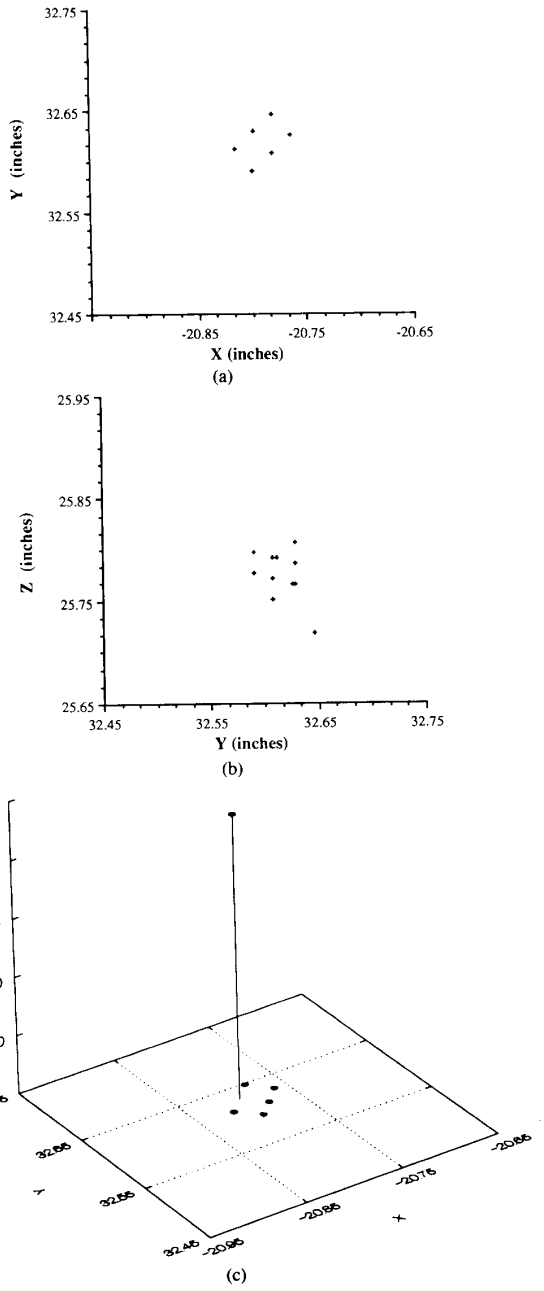

Fig. 10. (a) Scatter plots of the signal noise effects in the xy plane with a 40-Hz low-pass filter. (b) Scatter plots of the signal noise effects in the yz plane with a 40-Hz low-pass filter. (c) Histogram of (xy) plane with a 40-Hz low-pass filter.

Dynamic Testing

Two additional tests were implemented to test the system's performance. The first test considered a single pendulum supporting the eight targets on a 1.75-m bar. The resulting low-frequency motion covered an entire planar section of the target volume in an oscillatory pattern. Data were collected at frequencies from 60 to 480 Hz and showed, as expected, that there were no local discontinuities of global warping within the target volume.

The eight targets were placed at relatively regular intervals along the bar with the farthest being about 72 in from the pivot point. The targets were in a linear configuration to achieve the effect of concentric circles. The advantage of this configuration is that the angular position, with respect to the center (or the axis) of rotation, is the same for each detector. This fact was used in two separate analyses of the pendulum data.

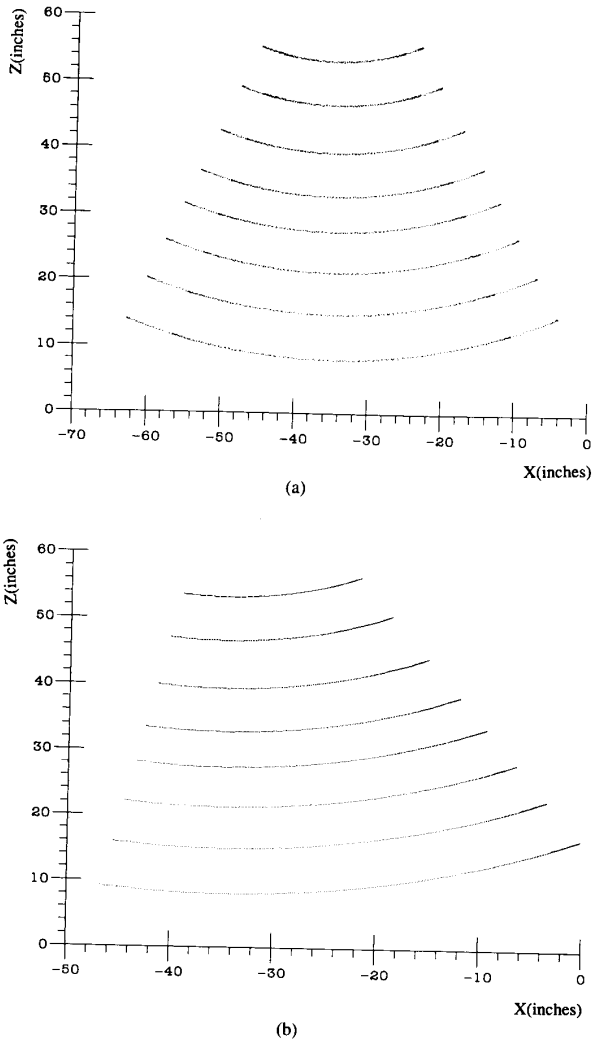

Fig. 11. (a) Cartesian position plot of the 120-Hz case. (b) Cartesian position plot of the 480-Hz case.

The first test was a simple plot of the points reduced from the timing data (no filtering). Since the motion was in the (xz) plane, only two axes were used for the plots. In the two cases displayed (Fig. 11), the sampling frequencies were 120 and 480 Hz. Other sampling rates were observed but, since the results were similar, only these two are shown. On these displacement records, the concentric arcs are clearly evident. At this point, inspection of these graphs tends to support that there are no irregularities in the target volume. Furthermore, the arcs traced out in the 480-Hz case are sharply defined and very smooth, which indicates that the signal noise is indeed small in the global sense. In the 120-Hz case, the arcs are still very smooth, but not as sharply defined. This is partly due to the longer sampling period and, thus, multiple swings of the pendulum. The dark spots are the locations where the pendulum changes direction; the deceleration followed by a reverse acceleration at the limits of its swing causes the sampling density to be higher in these locations. Since there is friction in the pin joint, there will be damping of the motion; this is reflected by the decreasing amplitude of each swing.

A second method of analyzing the pendulum data was to plot the computed angular position of each detector with respect to time. This method produced excellent results and is described in [17].

The second test was to determine performance under small displacement and high-frequency conditions. A single target was attached to the end of an aluminum rod, whose other end was mounted on the shaft of a closed-loop position controlled dc servomotor. The proportional controller applied an oscillatory signal to the target tipped rod at specified frequencies. Incorporated in the feedback loop was a high-resolution encoder, which provided an accurate angular displacement measurement independent of the MnScan generated data.

A more detailed description and analysis of this test in which the target was driven at frequencies from 0.5 to 25 Hz, and both the target photodetector and a shaft encoder were monitored, is also contained in [17].

Although further work is necessary, the implication thus far has been that this system can record higher frequency dynamic deflections which can be used for the dynamic analysis of manipulators or ultimately for closed-loop endpoint control.

Relative Orientation Between Robot Links

One of the motivations in developing this system is to measure the 3-D rotational and translational displacements of one body with respect to another. This information is significant to a number of areas, e.g., tracking the 3-D motion of human joints. It also has been shown that the dominant compliance in robots may come from the joints rather than from structural deflection in the links. Thus the system was used to determine the 3-D joint angles associated with relative motion of two bodies about a moving axis of rotation. These can be obtained based on the premise that three or more points define the position and orientation of a "rigid" robot link.

There are many ways of reducing sets of position data to orientation information, one of which is the SCHUT algorithm [7], [15], [16]. This is a least squares fit to a change in rigid body orientation. The result from the least squares fit is a quaternion expression which can be expressed in world coordinates as a relative change in position and orientation between two bodies. The method used in our system is quite similar, but instead of using the least squares technique, it averages the orientation to reduce error and to determine changes in orientation. The results from the two methods agree within 1° in most of the cases tested.

To check the accuracy in determining these angles, a single-degree-of-freedom jig was designed with each of the two links holding a cluster of four targets fixed with respect to each other. By displacing the jig throughout the measurement volume with the hinged joint angle fixed, the computed orientation angle based on the measured target locations can be compared to the actual angles. This was done for a range of

angles for each of the three planes. The results of this test placed the error of the measurement at $\pm 0.5°$ to $1.0°$ at the 95-percent confidence level. This represents the accuracy in predicting the relative orientation angle throughout the entire target volume for each of the three planes. Increasing the accuracy of the determination of the XYZ locations of targets and changing the relative locations of the targets in the cluster would improve the result significantly.

The additional calculation of the "instantaneous" axis of rotation of the joint in question is possible. Algorithms for this determination have been developed, with some being better than others [13].

An extensive analysis was performed on a) the effect of target xyz location accuracies, b) target detector topologies, c) tolerance errors in the relative locations of targets, and d) the effect of the algorithm itself on the accuracy of computing the position and orientation based on multiple target points attached in a rigid array to a body. The preliminary results which apply to many tracking systems were reported by Morris and Donath [12].

Conclusion

The system described provides a fast and accurate method to record human locomotion and end-effector motion parameters. The tests reported here were conducted on the initial prototype pending the imminent completion of a newer system. The earlier prototype is only capable of tracking eight targets; thus data are available only for one joint. The system displays good dynamic bandwidth and acceptable performance. Data collected for 1.75 s at 240 Hz for 2-limb segments in a human motion study (4 targets per limb) can be reduced to 3-D relative orientation or joint angles on our existing prototype in approximately 200 s (however, only 20 s are required for calculating the xyz coordinates of all eight points) on an Intel 8086 based system using code generated by a Fortran compiler (with no attempt at optimizing the code). This implies that a computation for a set of instantaneous orientation angles takes under 0.5 s (a 2.1-Hz rate), and the computation for the xyz coordinates of an individual target takes approximately 5.9 ms (168 Hz). The primary bottleneck is a computational one. A very preliminary test with an array processor has shown that the computational rates can be at least doubled. Significant improvements afforded by an array processor come about when large numbers of targets must be processed. Since this system was designed, new significantly faster CPU's have come to market which ought to speed up the computation further by between one and two orders of magnitude.

The accuracy of this system has surpassed the goal specification for human motion tracking for which it was originally designed; our goal had been to design a system with 0.1-in accuracy. The system in its present configuration is not yet sufficiently accurate for use as an endpoint sensor in the control of robot manipulators. However, we do feel that the system can already be used for facilitating quite a number of experiments in this field.

Although the system requires line of sight for operation, the number of light sources and detector targets can be increased to ensure line of sight in most instances. Furthermore, when obstructions to the line of sight are unavoidable, full recovery is achieved as soon as the obstructions are removed.

The resolution of the MnScan system is only a function of the system clock and laser scan speed. The errors that we have found are a function of a number of parameters including the accuracy in performing the calibration, some possible wobble in the motor shaft, the variation in the light's density profile across the plane's cross section, and the variation in the location on the photodetector's active area at which the target is triggered. Significantly better performance is planned for our next prototype.

Acknowledgment

The authors would like to thank T. Morris for repeating and confirming the test results reported in this paper.

References

[1] K. Antonsson and R. W. Mann, "Automatic 6-D.O.F. kinematic trajectory acquisition and analysis," *ASME J. Dyn. Syst. Meas. Contr.*, vol. III, no. 1, pp. 31–39, Mar. 1989.

[2] J. E. Bechtold, "Three-dimensional laser scanning system with application to gait and robotics," M.S. thesis, University of Minnesota, Aug. 1983.

[3] J. Chen and L. M. Chao, "Positioning error analysis for robot manipulators with all rotary joints," presented at the IEEE International Conf. on Robotics and Automation, San Francisco, CA, 1986.

[4] J. J. Craig, *Adaptive Control of Mechanical Manipulators*. Reading, MA: Addison-Wesley, 1988.

[5] A. Dainis and M. Juberts, "Accurate remote measurement of robot trajectory motion," presented at the IEEE Int. Conf. on Robotics and Automation, Saint Louis, MO, 1985.

[6] O. Khatib, "A unified approach for motion and force control of robot manipulators: The operational space formulation," *IEEE J. Robotics Automat.*, vol. RA-3, pp. 43–53, Feb. 1987.

[7] J. B. Lenox and J. R Cuzzi, "Accurately characterizing a measured change in confirguration," ASME paper 78-DET-50, 1978.

[8] J. F. Macfarlane, "A system for tracking motion in three-dimensional space," M.S. thesis, University of Minnesota, June 1983.

[9] J. F. Macfarlane and M. Donath, "Tracking robot motion in three-dimensional space: A laser scanning approach," in *Proc. NATO Advanced Study Institute on Robotics and Artificial Intelligence* (Italy, 1983); also in M. Brady, L. A. Gerhardt, and H. F. Davidson, Eds., *Robotics and Artificial Intelligence*. New York, NY: Springer-Verlag, 1985.

[10] W. Miller, III., "Sensor based control of robotic manipulators using a general learning algorithm," *IEEE J. Robotics Automat.*, vol. RA-3, pp. 157–165, Feb. 1987.

[11] B. W. Mooring and T. J. Pack, "Determination and specification of robot repeatability," presented at the IEEE Int. Conf. on Robotics and Automation, San Francisco, CA, 1986.

[12] T. Morris and M. Donath, "Error analysis of 6 D.O.F. rigid body motion tracking system," in *1988 Advances in Bioengineering*, G. R. Miller, Ed., BED-vol. 8. New York, NY: ASME.

[13] S. Peterson, "Kinematic analysis of the human joint," Ph.D. dissertation, Universtiy of Minnesota, Fall 1985.

[14] E. Schmitz and R. H. Cannon, "Further experiments in the end-point control of a flexible one link robot," to appear in *ASME J. Dyn. Syst. Meas. Contr.*

[15] G. H. Schut, "On exact linear equations for the computation of the rotational elements of absolute orientation," *Photogrammetrias*, vol. 17, no. 1, pp. 34–37, 1960–1961.

[16] ——, "Formation of strips for independent models," *Photgram. Eng.*, vol. 34, no. 7, pp. 690–695, July 1968.

[17] B. Sorensen, "A laser scanning system for tracking three dimensional motion of human gait," M.S. thesis, University of Minnesota, 1986.

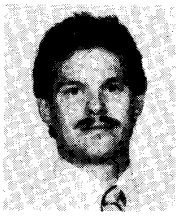

Brett R. Sorensen received the B.S. and M.S. degrees in mechanical engineering from the University of Minnesota, Minneapolis, in 1982 and 1986, respectively.

In 1985, he became a staff member at the Ballistics Research Laboratory in Aberdeen, MD, where he designs research ammunition for the army's battle tanks. Current interests are in automated design and design optimization of three-dimensional axisymmetric assemblies experiencing high stresses and strain rates.

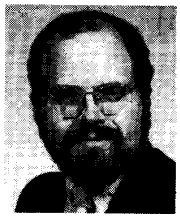

Max Donath (M'72) received the B.Eng. degree from McGill University, Montreal, Canada, in 1972 and the S.M., Mech.E., and Ph.D. degrees from M.I.T., Cambridge, MA.

He is currently Associate Professor of Mechanical Engineering at the University of Minnesota, Minneapolis, where he has been since 1978, except for 1986–1987 when he was a Visiting Associate Professor at Stanford University, Stanford, CA. His major research interests are in the mechanisms of integrating sensors, intelligence, and motor control function in order to provide the flexibility and adaptability associated with human capabilities. His research in the areas of walking and prosthetics, hand and arm control, sensor development, and autonomous navigation have implications to both industrial and rehabilitation activities. He has received a number of awards over the years, some of which include the Military order of the Purple Heart Award for Research for the Handicapped in 1981, the NSF Presidential Young Investigator Award, and the SME Young Manufacturing Engineer Award, both awarded in 1984. He is an Associate Editor of the *ASME Journal of Dynamic Systems, Measurement and Control.*

Guo-Ben Yang (S'87) received the Diploma in the Department of Mechanics from Zhejiang University, China, in 1970 and the M.S. degree in mechanical engineering from Oklahoma State University in 1984. He is currently completing the Ph.D. degree at the University of Minnesota, Minneapolis. His research interests include dynamics modeling and control of flexible robot manipulators.

Mr. Yang is a member of ASME.

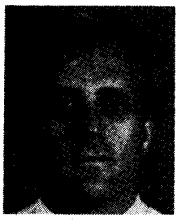

Roland C. Starr (M'88) received the B.A. degree in mathematics from Washington State University, Seattle, in 1979 and the M.S. degree in mathematics from the University of Minnesota, Minneapolis, in 1984.

Since that time, has has been pursuing the Ph.D. degree in mechanical engineering and working in the Motion Laboratory at Gillette Children's Hospital in St. Paul. His current research interest include kinematics, dynamics and control of walking machines, and the analysis of gait disorders in children with handicaps.

Mr. Starr is a member of the SIAM.